PAPER IN FOREFRONT

A combined chemical imaging approach using (MC) LA-ICP-MS and NIR-HSI to evaluate the diagenetic status of bone material for Sr isotope analysis

Anika Retzmann[1] · Magdalena Blanz[2,3] · Andreas Zitek[1,4] · Johanna Irrgeher[1,5] · Jörg Feldmann[3] · Maria Teschler-Nicola[6,7] · Thomas Prohaska[1,8]

Abstract

This paper presents a combination of elemental and isotopic spatial distribution imaging with near-infrared hyperspectral imaging (NIR-HSI) to evaluate the diagenetic status of skeletal remains. The aim is to assess how areas with biogenic $n(^{87}Sr)/n(^{86}Sr)$ isotope-amount ratios may be identified in bone material, an important recorder complementary to teeth. Elemental (C, P, Ca, Sr) and isotopic ($n(^{87}Sr)/n(^{86}Sr)$) imaging were accomplished via laser ablation (LA) coupled in a split stream to a quadrupole inductively coupled plasma mass spectrometer (ICP-QMS) and a multicollector inductively coupled plasma mass spectrometer (MC ICP-MS) (abbreviation for the combined method LASS ICP-QMS/MC ICP-MS). Biogenic areas on the bone cross section, which remained unaltered by diagenetic processes, were localized using chemical indicators ($I(C)/I(Ca)$ and $I(C) \times 10/I(P)$ intensity ratios) and NIR-HSI at a wavelength of 1410 nm to identify preserved collagen. The $n(^{87}Sr)/n(^{86}Sr)$ isotope signature analyzed in these areas was in agreement with the biogenic bulk signal revealed by solubility profiling used as an independent method for validation. Elevated C intensities in the outer rim of the bone, caused by either precipitated secondary minerals or adsorbed humic materials, could be identified as indication for diagenetic alteration. These areas also show a different $n(^{87}Sr)/n(^{86}Sr)$ isotopic composition. Therefore, the combination of NIR-HSI and LASS ICP-QMS/MC ICP-MS allows for the determination of preserved biogenic $n(^{87}Sr)/n(^{86}Sr)$ isotope-amount ratios, if the original biogenic material has not been entirely replaced by diagenetic material.

✉ Thomas Prohaska
   thomas.prohaska@unileoben.ac.at

1   Department of Chemistry, Division of Analytical Chemistry, VIRIS Laboratory, University of Natural Resources and Life Sciences, Vienna, Konrad-Lorenz-Str. 24, 3430 Tulln, Austria

2   Archaeology Institute, University of the Highlands and Islands, Kirkwall, Orkney KW15 1LX, UK

3   College of Physical Sciences, Department of Chemistry, Trace Element Speciation Laboratory Aberdeen (TESLA), University of Aberdeen, Meston Walk, Aberdeen AB24 3UE, UK

4   FFoQSI - Austrian Competence Centre for Feed and Food Quality, Safety & Innovation, FFoQSI GmbH, Technopark 1C, 3430 Tulln, Austria

5   Institute of Coastal Research, Marine Bioanalytical Chemistry, Helmholtz-Zentrum Geesthacht, Max-Planck Str. 1, 21502 Geesthacht, Germany

6   Department of Anthropology, Museum of Natural History, Burgring 7, 1010 Vienna, Austria

7   Department of Evolutionary Anthropology, University of Vienna, Althanstrasse 14, 1090 Vienna, Austria

8   Chair of General and Analytical Chemistry, Montanuniversität Leoben, Franz Josef Str. 18, 8700 Leoben, Austria

Abbreviations

ICP-QMS	Inductively coupled plasma quadrupole mass spectrometer
LA	Laser ablation
LASS ICP-QMS/ MC ICP-MS	Laser ablation coupled via a split stream to a quadrupole inductively coupled plasma mass spectrometer and a multicollector inductively coupled plasma mass spectrometer
MC ICP-MS	Multicollector inductively coupled plasma mass spectrometer
NIR	Near-infrared
NIR-HSI	Near-infrared hyperspectral imaging
PCA	Principal component analysis
ROI	Region of interest

Introduction

The investigation of provenance and migration of past humans and animals is of substantial interest in anthropological and archeological research. Recent developments in analytical chemistry allow "reading" the incorporated chemical fingerprint in skeletal remains, which can be correlated to the individual's region of origin. In this context, strontium (Sr) isotope ratio analyses of human and animal skeletal remains to trace residential changes and/or living conditions by either thermal ionization mass spectrometry (TIMS) or MC ICP-MS have evolved as key tools in anthropology and archeology, as comprehensively described in recent reviews [1–4]. To minimize damage to valuable remains, and to investigate the spatial resolution of the incorporated Sr signature (e.g., growth layers of tooth enamel), LA as a direct sample introduction system has been coupled to a (MC) ICP-MS [5–12]. For migration studies, the main interest lies in the $n(^{87}Sr)/n(^{86}Sr)$ isotope-amount ratio, which varies according to the radioactive decay of ^{87}Rb to ^{87}Sr (half-life $\sim 48.8 \times 10^9$ years) and is therefore a function of the geological age and the original Rb/Sr ratio [13]. (In this manuscript, the isotope-amount ratio notation (e.g., $n(^{87}Sr)/n(^{86}Sr)$) follows IUPAC guidelines according to [14].) Sr is released via weathering from the bedrock material, and due to its chemical similarity to Ca, it is taken up by and incorporated into plants and animals. It is finally taken up by animal and human organisms as a substitute for Ca, mainly incorporated in hard tissues (teeth and bones) [1]. Since no significant fractionation of the environmental $n(^{87}Sr)/n(^{86}Sr)$ isotope signature occurs during the biological uptake [13, 15], the incorporated radiogenic Sr isotopic signature reflects the ratio of a particular geographic location inhabited during a specific period of an individual's life, depending on the type of tissue and its specific turnover [1, 13]. In this context, tooth enamel has been shown to act as an "archive of the childhood" [5] of the Sr uptake in an individual's life, as tooth enamel reflects the Sr signature of the years of life when mineralization takes place (incremental growth of human third molar enamel continues until completion between 12 and 16 years of age [2]). Contrary to tooth enamel, dentin and bone tissue undergo continuous turnover during life and therefore reflect the Sr isotope signature of the last 10 to 20 years of an individual before death [2, 3]. The comparison of the $n(^{87}Sr)/n(^{86}Sr)$ isotope-amount ratio within tooth enamel and bone/dentin has been successfully applied to reconstruct the past (migration and diet) of past individuals [16–21]. In instances where (multiple) migration took place within months or a few years prior to death of an individual, the "multi-year archives" [20] of bones might be reconstructed by analyses of multiple bones types, which vary in bone turnover and thus also carry different Sr archives [2]. For example, the $n(^{87}Sr)/n(^{86}Sr)$ isotope-amount ratios within the femur and the rib of "Ötzi," the Tyrolean Iceman, potentially indicate multiple changes in (residential) localities during the last years of his life [22].

The post-depositional overprint of the Sr isotopic signatures in ancient skeletal remains by cumulative physical, chemical, and biological alteration in the form of inorganic modifications and structural alterations—referred to as diagenesis—is a challenge in the application of the technique and the interpretation of results [23]. Diagenetic Sr from soil moisture and groundwater of the burial environment accumulates post mortem in the archeological bone due to recrystallization of the hydroxyapatite lattice, adsorption onto the apatite crystal surface, and crystallization of secondary minerals (e.g., brushite ($CaHPO_4 \cdot 2H_2O$) or carbonate ($CaCO_3$)) in micro-cracks, pores, and vacancies [5, 24–27]. This diagenetic effect may alter the Sr fingerprint, shifting it away from that incorporated in vivo (often referred to as biogenic Sr signal). Studies by Kyle [28] showed that archeological tooth enamel is well preserved in contrast to bones and dentin due to its extremely compact structure with very little pore space and minor amounts of organic content ($\sim 2\%$). Hence, tooth enamel has been a preferred sample for Sr isotopic analysis. Dentin and bone material on the other hand with their higher porosity, smaller crystallites and a higher organic content ($\sim 30\%$) show a stronger susceptibility to diagenetic changes [29]. Nonetheless, the combination of the incorporated childhood signature in tooth enamel with the incorporated isotopic signature of the last 10–20 years before death in dentin and bone allows for a more substantial reconstruction of the past movement pattern of an ancient individual [2, 3]. Furthermore, in certain archeological/anthropological contexts non or only little dental tissue is preserved, wherein migratory information has to be extracted from bone tissue. Therefore, a diligent assessment of the diagenetic process is a prerequisite to avoid scientific conclusions drawn from insufficiently preserved material and rigorous methods to assess the biogenic signal are mandatory.

A major concern is the fact that soil water can penetrate through the porous structure (caused e.g. by the Haversian channels and bone canaliculi) deeply into the inner parts of the cortical bone and cause diagenetic changes. In order to retrieve the biogenic signal from bone and dentin, several protocols have been established: Sample preparation included for example mechanic abrasion of the outer bone/dentin surfaces to remove diagenetically altered material [30]. The procedure significantly reduced the content of Zn, Cd, K, Al, Fe, and Mn but showed no effect for the diagenetic impact of Na, Ca, Mg, Sr, and Ba [31]. Other protocols were based on acid wash procedures to remove the high soluble diagenetic bioapatite from archeological remains, by significantly reducing the contamination level and revealing the theoretical w (Ca)/w(P) mass fraction ratio of modern bones. However, the original biogenic $n(^{87}Sr)/n(^{86}Sr)$ isotope-amount ratios could not be recovered [31].

The solubility profiling method has been applied to retrieve the biogenic fraction in bulk bones. The method is based on sequential leaching of bone/dentin powder using acidic acetate buffer and allows for the isolation of biogenic bone leaching fractions with w(Ca)/w(P) mass fraction ratio close to the theoretical value of biogenic hydroxyapatite (2.16) and a stable w(Sr)/w(Ca) mass fraction ratio based on the differing solubility of diagenetic bioapatite (carbonate and fluoride content among others) [32]. This enables the identification of leaching fractions containing biogenic $n(^{87}Sr)/n(^{86}Sr)$ signatures which may be used to ascertain the geographic origin of the individual. However, the numerous leachates required to remove Sr in secondary minerals and from surface absorption make the method time-consuming and only applicable for solution-based analysis. The method of solubility profiling is limited in revealing biogenic $n(^{87}Sr)/n(^{86}Sr)$ signatures when chemical changes altered the original bioapatite crystal structure [24, 27, 32].

In population studies, the correlation of the Sr mass fraction w(Sr) and the $n(^{87}Sr)/n(^{86}Sr)$ isotope-amount ratios in bone/dentin in combination with the chemical information of the burial environment was applied as a useful tool to assess a potential diagenetic impact [9, 27] following the routine approach used for C and N isotopes in collagen [33].

Beside the mentioned methods to monitor diagenesis for solution-based analysis of bone/dentin, several studies applied chemical imaging techniques to assess the extent of diagenetic alterations. These investigations have become necessary as spatial information is a substantial information pool. Herein, trace element mass fractions and diffusion gradients (mainly REE, Y, Hf, U, Th) [34–38] are monitored as sensitive tracers for diagenetic processes that take place shortly after the death of the individual, since they occur in fresh bone and tooth material at very low concentration levels [20, 25, 33]. Especially REE pattern reflects different diagenetic processes with associated fractionation and diffusion profiles [33].

Furthermore, Willmes et al. [38] developed a less-destructive depth-profile scanning method using LA-ICP-MS based on the clear correlation between distribution of diagenetic U and diagenetic Sr revealed by chemical imaging of U and Sr on Neanderthal teeth cross sections. The monitoring of trace element mass fractions has also been applied in solution-based analysis [20, 25].

Punctual X-ray diffraction (XRD) and mid-infrared spectroscopy (MIR, approx. wavelength between 2500 nm ($\triangleq 4000$ cm^{-1}) and 25,000 nm ($\triangleq 400$ cm^{-1})) methods such as Fourier transform infrared spectroscopy (FTIR) have been widely applied to characterize the preservation of bone and dentin. Herein, the crystallinity index (CI) [39] as a splitting factor between the two phosphate ion absorption peaks (605 cm^{-1} ($\triangleq 16,530$ nm) and 565 cm^{-1} ($\triangleq 17,700$ nm)) quantifies the increase in crystallinity of bioapatite structure due to the loss of collagen and the post-depositional recrystallization of calcium phosphate [21, 26, 40–43]. The divergent total carbonate content (C/P index) estimated via the ratio of the absorption peaks a (CO$_3^{2-}$; 1415 cm^{-1} ($\triangleq 7070$ nm))/a (PO$_4^{3-}$; 1035 cm^{-1} ($\triangleq 9660$ nm)) correlates with the precipitation of secondary carbonates and their surface adsorption [26, 42, 43]. The authigenic calcite calculated semi-quantitatively via the height of the absorption peak at 713 cm^{-1} ($\triangleq 14,025$ nm) in comparison to a reference material [44] indicates the presence of diagenetic modification [21]. The mineral-to-matrix ratios calculated from integrated areas of phosphate bands (900–1200 cm^{-1} ($\triangleq 11,110$–8330 nm)) to amide I bands (1585–1720 cm^{-1} ($\triangleq 6310$–5850 nm)) [45] indicate large amounts of preserved collagen in bones [21].

First studies applied non-destructive spectroscopic imaging techniques such as mid-infrared [46, 47], near infrared (NIR) [48, 49], and hyperspectral near-infrared [50, 51] imaging (NIR-HSI, approx. wavelength between 400 nm ($\triangleq 25,000$ cm^{-1}) and 2500 nm ($\triangleq 4000$ cm^{-1})) for monitoring the general preservation of forensic and archeological remains as well as differentiation between remains in soil samples. These spectroscopic imaging outperform the classical MIR and NIR techniques by providing spatial and spectral resolution covering the heterogeneity information of samples, while requiring minimal sample preparation [50, 52]. In general, the passive remote sensor system of HSI digitizes the electromagnetic radiation (reflectance and emission) of an object in a variety of adjacent spectral bands (VIS and IR) which can be described as a three-dimensional data cube with the spatial extensions x, y and the third dimension λ, representing the spectral dimension. Hence, each pixel of an HSI image of a tooth/bone contains an absorption spectrum (spectral signature) based on the mineralogical/chemical composition of the displayed material in a certain position [53]. In comparison to NIR imaging, NIR-HSI measures energy in narrower and more numerous bands (> 20), which provides

a continuous spectral measurement across the near-infrared spectrum [54]. Via classification of these pixels by e.g. principal component analysis (PCA), mineralogically/ chemically different regions can be identified, which holds on great potential for diagenetic studies.

The problem of diagenesis has been known, discussed and investigated for more than 30 years, and several methods have been developed and applied. Still, there is no fully satisfactory method to assess the overall diagenetic status of archeological remains and to monitor diagenetically changed regions for a reliable evaluation of (pre-)historic migration (paths). A well-preserved biogenic Sr signal is indispensable when using $n(^{87}Sr)/n(^{86}Sr)$ isotope-amount ratios analysis to determine (pre-)historic migration (paths). Herein, we present for the first time the combination of elemental and isotopic imaging with near-infrared hyperspectral image analysis, cross-referenced with results from sequential bone leaching of the same samples, to identify and subsequently assess biogenic regions. These data will aid in the development of hyperspectral imaging as a cheap and fast method of scanning bones to identify best preserved areas of bones, which may then be selectively targeted for $n(^{87}Sr)/n(^{86}Sr)$ analysis. This would allow for the routine analysis of only partially preserved bones, and potentially obviate the need for lengthy solubility profiling methods to identify biogenic Sr signals. The approach has a substantial potential to allow for the spatial determination of the biogenic $n(^{87}Sr)/n(^{86}Sr)$ isotopic signature in skeletal remains for a reliable interpretation of analytical datasets and the reconstruction von residential changes or diet and nutrition habits of ancient human and animals.

Experimental

All preparatory laboratory works were performed in a clean room (ISO class 8 according to ISO 14644-1). Type I reagent-grade water (18 MΩ cm) (F + L GmbH, Vienna, Austria) was further purified by sub-boiling distillation (Milestone-MLS GmbH, Leutkirch, Germany). Nitric acid was prepared by double sub-boiling distillation of analytical reagent-grade acid (65% w/w) (Merck KGaA, Darmstadt, Germany). All polyethylene (PE) flasks, tubes, and pipette tips (VWR International GmbH, Vienna, Austria), as well as perfluoroalkoxy (PFA) screw cap vials (Savillex, Minnetonka, USA), were cleaned in a two-stage washing procedure using nitric acid (10% w/w and 1% w/w) and were then rinsed with Type I reagent-grade water before use.

Preparation of human femur samples

Two intact human femurs (sample ID ES_SK91 and GT_25.025) recovered from two archeological sites in Austria (ES, Elisabethstrasse, Vienna; GT, Gars/Thunau, Lower Austria) were provided by the Museum of Natural History, Vienna. The specimens were selected for their purported different state of diagenetic alterations based on their different localities and absolute ages (fourteenth century AD, ninth century AD) (see Table 1).

From each bone, a section of about 5 × 3 × 1 cm was taken by partially cross-sectioning along the bone shaft of the femurs (see Electronic Supplementary Material (ESM) Fig. S1). The bone samples were cleaned by ultrasonicating (Bandelin Sonorex Digitec Ultrasonic Bath DT 255, Bandelin electronic GmbH & Co. KG, Berlin, Germany) in high-quality water (0.06 μS cm^{-1}) from a TKA GenPure water treatment system (TKA Wasseraufbereitungssysteme GmbH, Niederelbert, Germany) for 10 min and dried at 40 °C until constant weight. These bone pieces were subsampled further for the present study.

Bone cross sections for chemical imaging

Following cleaning, two 1–1.5-mm-thick cross sections perpendicular to the length of the bone shaft were obtained using a low speed saw (IsoMet, Buehler, Lake Bluff, IL, USA) with a diamond-rim blade (Series 15LC IsoMet Wafering Blade, Buehler). The cross sections were cleaned using high-quality water and air-dried. One cross section of each bone was fixed using double-sided adhesive tape onto a glass plate of the size of the ablation chamber (10 cm × 10 cm) for the LASS ICP-QMS/MC ICP-MS measurements. The opposite cross section of each bone was fixed using double-sided adhesive tape onto an object glass slide for NIR-HSI measurements.

Table 1 List and key characteristics of bones investigated in this study; both samples originate from the shafts of human femurs

Sample ID	Origin	Sex	Approx. age	Approx. time of death
ES_SK91	Excavation Elisabethstraße, Vienna, Austria	Female (?)	30–40 years	14th century AD
GT_25.025	Excavation Gars-Thunau, Lower Austria, Austria	Inconclusive*	40–55 years	9th century AD

*No sex determination possible

Bone powder for solubility profiling

Powder samples of cortical bone adjacent to the cross sections were obtained from the dry bone samples using a Dremel Moto 396 Type 1 drill with a diamond drill bit (Dremel Manufacturing Co., Racine, WI, USA). In order to limit the damage, only one sample of about 50 mg was obtained per bone, for each of which a fresh drill bit was used.

Near-infrared hyperspectral image analysis

Near-infrared hyperspectral images were recorded using a push-broom HSI instrument (Zeutec Gmbh). The instrument is equipped with a Xenics NIR camera (Xeva-USB-FPA-1.7-320-TE1-100 Hz; XEVA 6179; 0.9 to 1.7 μm; 320 × 256 pixel matrix; 12 bit) operating an InGaAs focal plane array sensor with 2% pixel noise. The camera is connected to a Specim N17E spectrograph (Spectral Imaging Ltd., Oulu, Finland) operating in the wavelength range of 900–1700 nm with 5-nm spectral resolution, with an objective lens (2/3" C-mount broadband coated lenses, Schneider–Kreuznach CINEGON). The system consists of a 600-mm y-table gear and stable diffuse 45/0 illumination created by halogen bulbs emitting light of the entire spectral range of the spectrograph. The y-table was driven by Isel LF4 mechanics and an Isel TMO-4403 (PICMIC) stepping motor controlled by textual commands via an RS-485 interface. A forced convection (TE-1) cooling was applied to cool down the XEVA 6179 camera to a temperature between − 4 and − 13 °C, which is needed to reduce the noise in the images. The field of view for the samples was selected by setting the appropriate height of the spectrograph in relation to the sample. Image focusing was achieved by adjusting the lens. The setup of the optics resulted in a resolution of 0.156 mm/pixel. The image processing system and the sensor were controlled using Argus software [55].

Before measurement, a two-point calibration was carried out using a diffuse reflectance standard (Sphereoptics) as a "white reference" and by completely covering the objective lens for a "black reference." Relative reflectance (R) of the sample image ("x") to the black ("min") and white ("max") reference was calculated as shown in Eq. 1, using Argus software [55]. The two bones were analyzed by NIR-HSI on the mirroring thin section of those analyzed by laser ablation.

$$R = \frac{x - min}{max - min} \qquad (1)$$

Before analyzing the data cube, dead pixels were removed using a machine-specific in-house MatLab algorithm. The subsequent analysis of the data cube was carried out using the MatLab-based PLS Toolbox of Eigenvector Research Incorporated (Manson, USA). Data were pre-processed using Sawitzky-Golay smoothing (Polynomial Order 1, Derivative Order 1) with subsequent median centering of spectra after background removal. Finally, a PCA overall data points from both bone samples (EK_SK91 and GT_25.025) together was conducted, and loading plots and plots of the principal components were produced. The loading plots were used to identify the most relevant wavelengths for the discrimination of zones with different chemical compositions, and images of slabs of relative reflectance of the selected significant wavelengths were produced.

Images were exported from PLS toolbox as TIFF-files with 600-dpi resolution and at a size similar to the size of the microscope images of the ablated samples for optimizing matching for further processing of spectral image slabs at selected wavelengths (1410 nm and 1150 nm).

Elemental and isotopic imaging

LASS ICP-QMS/MC ICP-MS measurements

A nanosecond excimer-based laser ablation system (NWR 193, ESI-NWR Division, Electro Scientific Industries, Inc., Portland, CA, USA) was coupled to an ICP-QMS (NexION 350D, Perkin Elmer, Waltham, MA, USA) and a MC ICP-MS (Nu Plasma HR, Nu Instruments, Wrexham, UK) using a split-stream laser ablation setup following the protocol of Prohaska et al. for the simultaneous detection of the multi-elemental composition (C, P, Ca, Sr) and $n(^{87}Sr)/n(^{86}Sr)$ isotope-amount ratio data of the bone samples [56]. General instrumental settings for the LASS ICP-QMS/MC ICP-MS are described in ESM Table S1.

Sr isotopic data were collected using static multicollection with an integration time of 0.2 s using the corresponding detector configuration as shown in ESM Table S2. A solution of NIST SRM 987 (highly purified $SrCO_3$, NIST, Gaithersburg, USA) [57] with a mass fraction of approximately 50 ng g^{-1} was introduced as bracketing standard via an Aridus II (Cetac Technologies, Omaha, NE, USA) desolvating nebulizer for optimization and correction of instrumental isotopic fractionation (IIF) at the beginning and end of each laser ablation event in the following sequence: liquid standard1—laser ablation solid sample—liquid standard2. During laser ablation, dual sample introduction to the MC ICP-MS from the laser and a dry solution aerosol of 2% (w/w) nitric acid by an Aridus II (Cetac Technologies) desolvating nebulizer was performed to minimize changes in plasma conditions according to Prohaska et al. [56].

Laser ablation was performed in line scans from the inner core to the outer rim area of each bone sample. Both the ICP-QMS and the MC ICP-MS were set to record time-resolved signals, with 2.27 data points recorded by the MC ICP-MS for every data point recorded by ICP-QMS (integration time of 0.453 s). A gas blank of 100 s was recorded at the beginning

of each measurement. Since the detection range of the MC ICP-QMS is limited, laser settings were tested for each bone prior to analysis, and adjusted as needed to obtain similar signals for both bones (see ESM Table S1).

In-house pressed reference pellets of NIST SRM 1400 and NIST SRM 1486—certified for P, Ca, and Sr; values for $n(^{87}Sr)/n(^{86}Sr)$ isotope-amount ratios have been determined in several studies [58–60]—were measured using line measurements under similar conditions as the samples at the beginning and end of each laser ablation event for quality control and correction of polyatomic interferences.

Data evaluation and reduction

The average gas blank values were subtracted from the measured values of the samples for each measurement.

Multi-elemental dataset All measured intensities of ^{12}C, ^{31}P, and ^{88}Sr were normalized to ^{43}Ca. Additionally, measured intensities of ^{12}C and ^{43}Ca were normalized to ^{31}P. On the basis of the Ca-normalized ^{88}Sr intensities, the mass fractions of Sr were determined applying a one-point calibration using certified Sr mass fractions of NIST SRM 1400. The $w(Sr) \times 1000/w(Ca)$ mass fraction ratios were calculated under the assumption of the presence of pure bioapatite ($w(Ca) = 0.4$). The $w(Ca)/w(P)$ mass fraction ratios were calculated based on the certified $w(Ca)/w(P)$ values of NIST SRM 1400 and NIST SRM 1486. Since the C mass fractions of the NIST SRM 1400 and NIST SRM 1486 are not certified, $I(C) \times 10/I(P)$ and $I(C)/I(Ca)$ intensity ratios were calculated instead of C mass fractions to identify regions with increased C levels.

Sr isotope dataset Data correction of the Sr isotope dataset was accomplished according to [61, 62]: Gas blank correction, correction of the ^{87}Sr signal by subtraction of the ^{87}Rb signal (obtained from ^{85}Rb via the natural abundance ratio of $n(^{87}Rb)/n(^{85}Rb)$, and using the certified $^{88}Sr/^{86}Sr$ ratio of the NIST SRM 987 standard solution for IIF correction) [56, 61, 62], a correction for the contributions of calcium dimers and argides [61, 62], a correction for the contribution of $^{40}Ca^{31}P^{16}O^+$ and $^{40}Ar^{31}P^{16}O^+$ polyatomic clusters (incorporating $^{88}Sr/^{43}Ca$ data from the ICP-QMS data for a dynamic correction) [7, 61, 62], and external IIF correction of the $n(^{87}Sr)/n(^{86}Sr)$ isotope-amount ratio using the NIST SRM 987 bracketing standard [56]. Corrections for doubly charged rare earth elements were not performed, as values at m/z 85.5, 86.5, and 87.5 were at blank level.

Image creation and statistical analysis

Microscope images of the bone samples were taken after laser ablation including a spatial scale using a standard binocular microscope (S63T Trinocular Pod 8-50x) connected to a

digital camera (ProgRes CT3, Jenoptik, Jena, Germany) in 8- to 10-fold magnification. The microscope images were imported and georeferenced in the geographical mapping software ArcGIS® 10.4.1 (ESRI, Redlands, CA, USA) by using the spatial reference scale, which creates a spatial reference system for the images. The laser ablation lines were digitized and the x-y coordinates of the start and end points of each line were determined. By knowing the distance between the first and last data point in x and y direction and the amount of data point in between, the intermediate x- and y-coordinates for each data point (z-values) were calculated according to Draxler et al. [63]. These data (including multi-elemental and Sr isotope ratio data) were then imported to ArcGIS® as an overlay to the microscopic images.

The relative reflectance images from near-infrared hyperspectral image analysis at the selected wavelengths (1410 nm and 1150 nm) were also imported to ArcGIS® and referenced manually to the elemental and isotopic images/datasets. Subsequently, the data from the spectral raster images were extracted to the laser ablation data points using the Spatial Analysis Tool "Extract Multi-Values to Points" of ArcMap.

The merged datasets were exported in DBF format for further processing using MS EXCEL®. Since elemental, isotopic, and near-infrared hyperspectral data were gathered with different spatial densities and in order to reduce the complexity of these data, all three datasets were buffered according to the applied spot size (100 μm and 150 μm), by calculating their average. Each data point displayed in the resulting chemical images of the bone sample ES_SK91 (diameter of 100 μm) contains 22 elemental ratio or mass fraction data points and 50 Sr isotope ratio data points, whereas each data point in the chemical images of the bone sample GT_25.025 (diameter of 150 μm) contains 33 elemental ratio or mass fraction data points and 75 isotopic data points (see ESM Table S1).

To allow for an intersample comparison of the elemental, isotopic, and near-infrared hyperspectral data, the buffered data were re-imported into ArcGIS® and the coloration of data points was set by classes evenly distributed in the range of data values. Chemical images for relative reflectance at wavelength 1410 nm, $w(Sr) \times 1000/w(Ca)$ mass fraction ratios, $w(Ca)/w(P)$ mass fraction ratios, $I(C) \times 10/I(P)$ intensity ratios, $I(C)/I(Ca)$ intensity ratios, and $n(^{87}Sr)/n(^{86}Sr)$ isotope-amount ratios were created. Further details on the creation of spatial images using the software tools of ArcGIS® are published elsewhere [56, 63, 64].

Selection of regions of interest Regions of interest (ROIs: outer rim, inner core, preserved collagen, and transition area) were defined and digitized in ArcGIS® in order to differentiate between diagenetically altered and diagenetically unaltered areas on the bone sections and to allow for further

(statistical) interpretation of the datasets. The boundaries of these areas were determined for each bone section individually based on chemical distribution patterns of $w(Ca)/w(P)$ and $w(Sr) \times 1000/w(Ca)$ mass fraction ratios, $I(C) \times 10/I(P)$ and $I(C)/I(Ca)$ intensity ratios, and the relative reflectance at wavelength 1410 nm. Additional visible inspection of the histological characteristics was accomplished by light microscopy. The digitized ROIs were assigned to the elemental, isotopic, and near-infrared hyperspectral data by intersecting their information layer in ArcGIS®. The merged datasets were exported in DBF format for further statistical processing using PASW 18® (Armonk, NY, USA).

The export of the measured and quantified data of the corresponding ROIs from ArcGIS® allowed for a comparative statistical evaluation of the data and the associated ROIs using PASW 18®. An overview table displaying intensity of reflection on selected wavelengths, elemental, and Sr isotope ratio distribution within the different ROIs (outer rim area, preserved collagen, transition area, inner core area) given as percentile (5%, 25%, 75%, and 95%), median, and mean was created for both bone samples.

Solubility profiling

Bone powder samples were leached with 0.1 mol L^{-1} acetic acid/sodium acetate buffer with a pH of 4.5 following a 30-step in-house optimized protocol based on [65, 66] modified from the sequential leaching procedure presented by Sillen [32]. Multi-elemental analysis was performed using the ICP-QMS (NexION 350D, Perkin Elmer) with an Ar plasma in standard mode to determine P, Ca, and Sr mass fractions of leachate aliquots using external calibration (ICP multi-element standard solution VI, Merck; rare earth multi-element solution ESI-71, Elemental Scientific, Omaha, NE, USA; single-element standard of phosphorus, Inorganic Ventures, Christiansburg, VA, USA) and internal normalization (single element standard of indium, Merck). General instrumental settings for the multi-elemental measurements are described in ESM Table S4. The total mass fractions of leached P, Ca, and Sr of powdered samples were determined. Based on these, $w(Sr) \times 1000/w(Ca)$ and $w(Ca)/w(P)$ mass fraction ratios were calculated.

In order to allow for sufficient signal intensity in Sr isotope ratio measurement, every three successive leachates of the 30 total leachates from each sample were pooled, resulting in 10 pooled leachates (with the exception of the initial three leachates (see EMS Table S5 for more details)), evaporated, and re-dissolved in 2 mL of 8 mol L^{-1} nitric acid. Prior to Sr isotope ratio analysis, Sr/matrix separation was performed according to the methods described in Swoboda et al. [67] and Irrgeher et al. [68] for all pooled leachate samples, blanks, and including Sr isotopic certified reference material NIST SRM 987.

The $n(^{87}Sr)/n(^{86}Sr)$ isotope-amount ratios of the pooled leachates were measured using a MC ICP-MS (Nu Plasma HR, Nu Instruments) equipped with a desolvation nebulization membrane unit (Aridus II, Cetac Technologies) in combination with a PFA nebulizer (Microflow ST Nebulizer, Elemental Scientific) as a sample introduction system. (Operating conditions see ESM Table S6.) Pooled leachates were diluted with nitric acid (2% w/w) after separation to achieve a mass fraction of 50 ng g^{-1}. A solution of NIST SRM 987 with a mass fraction of 50 ng g^{-1} was used as an isotopic reference for standard-sample bracketing (SSB). Diluted leachates and NIST SRM 987 solution were spiked with Zr (Merck) to allow for internal inter-elemental IIF correction of time-dependent and matrix-dependent variation between the samples. A detailed description of the general instrumental settings, data collection, blank correction, and measurement strategy for the $n(^{87}Sr)/n(^{86}Sr)$ isotope-amount ratio measurement can be found in Retzmann et al. [69]. Data processing and uncertainty calculations were performed following standard protocols [70, 71]. Further detailed information on the analytical procedures of solubility profiling can be found in ESM Method.

Determination of biogenic Sr signatures

In accordance with the pattern of $w(Ca)/w(P)$ mass fraction ratios observed by Sillen [32] and previous in-house studies [65, 66], the first and second pooled leachates were excluded from the determination of biogenic $n(^{87}Sr)/n(^{86}Sr)$ isotope-amount ratios since they bear elevated $w(Ca)/w(P)$ mass fraction ratios, which predominantly contain material low in phosphorous (e.g., calcites), wherein the corresponding $n(^{87}Sr)/n(^{86}Sr)$ isotope-amount ratios are likely not representative of biogenic values. The pooled leachates 3 to 6 were excluded from the determination of biogenic $n(^{87}Sr)/n(^{86}Sr)$ isotope-amount ratios since they bear elevated $w(Sr) \times 1000/w(Ca)$ mass fraction ratios compared to elemental mass fractions observed in biogenic material [1, 72], which indicate diagenetic Sr incorporated into the recrystallized bone. Small decreases of $w(Sr) \times 1000/w(Ca)$ mass fraction ratios < 21% from pooled leachate 7 onwards are considered as stable and representing the biogenic fractions [32]. Since the extent of diagenetic alteration varies between samples, the selection of the leachates for the determination of biogenic $n(^{87}Sr)/n(^{86}Sr)$ isotope-amount ratios was assessed on an individual basis [27]: In the case of the bone sample ES_SK91 (approx. time of death fourteenth century AD), where the later leachates display constant $n(^{87}Sr)/n(^{86}Sr)$ values, the average of pooled leachates 7 to 11 was taken to determine the biogenic $n(^{87}Sr)/n(^{86}Sr)$ isotope-amount ratios. In the case of the bone sample GT_25.025 (approx. time of death ninth century AD), where the $n(^{87}Sr)/n(^{86}Sr)$ isotope-amount ratio of the pooled leachates 7 to 11 displays a near linear decrease in value, pooled

leachate 11 was considered to be the closest approximation of the biogenic $n(^{87}\text{Sr})/n(^{86}\text{Sr})$ isotope-amount ratios, though it may well be even lower. Further detailed information and discussion on the determination of biogenic $n(^{87}\text{Sr})/n(^{86}\text{Sr})$ isotope-amount ratios from solubility profiling can be found in ESM Discussion.

The biogenic $n(^{87}\text{Sr})/n(^{86}\text{Sr})$ isotope-amount ratios determined by solubility profiling from bulk samples (adjacent to cross sections) were used as reference values for the biogenic $n(^{87}\text{Sr})/n(^{86}\text{Sr})$ isotope-amount ratios determined by LA MC ICP-MS measurements and therefore served to validate the effectiveness of the determination of biogenic areas using LASS ICP-QMS/MC ICP-MS and NIR-HSI.

Results and discussion

Near-infrared hyperspectral imaging

PCA overall data points together gathered from the near-infrared hyperspectral images of the cross sections (opposite to those used in LA (MC) ICP-MS analysis) from both bone samples (EK_SK91 and GT_25.025) shows that the first two components explain more than 85% (PC1–2, 73% and 12%) of the variation in the data (see Fig. 1a). The analysis of the loading for PC1 indicates two wavelengths of influence at 1150 nm and 1410 nm (see Fig. 1b). A similar loading of PC1 for wavelength 1410 nm at half the extent and a tenth of the extent for wavelength 1150 nm was reported by Vincke et al. [51] when analyzing bone specimens to identify overall sufficient collagen for ^{14}C dating using accelerator mass spectrometry. They excluded the wavelength 1410 nm as indicator of O–H bonds which may be linked to carbonated crystal apatite or water content and used wavelength 1430 nm (N–H first overtone) instead, which was identified in PC2 loading.

In contrast, Stathopoulou et al. [48] and Thomas et al. [49] attributed the wavelength 1432 nm to the overtone of the fundamental OH$^-$ mode, which proved to be a property of biogenic apatites [48]. Therefore, the wavelength of influence at 1410 nm was utilized in the present approach to identify biogenic apatites.

Figure 2b and c shows the reconstructed image slabs of relative reflectance at the wavelengths of influence 1410 nm and 1150 nm identified by the first principal component, whereas the coloring indicates differences in the score values, suggesting changes in physical and chemical compositions of the bones. While bone sample GT_25.025 shows a mainly homogenous coloring with just slight differences, bone sample ES_SK91—especially in the center area where preserved collagen is likely present—displays a large extent of coloring differences in the intra-bone and inter-bone comparison to GT_25.025.

Identification of areas of preserved biogenic bone material

Figure 3a shows the spot size-buffered line plots of the relative reflectance at wavelength 1410 nm together with the intensity ratios $I(\text{C})/I(\text{Ca})$ and $I(\text{C}) \times 10/I(\text{P})$ of bone sample ES_SK91. The center of the bone cross section with likely preserved collagen in biogenic apatite present (according to blue coloring in the image slab, Fig. 2) displays a relative reflectance lower than 150 at wavelength 1410 nm (between 1650 and 4250 μm distance in the line plot, see Fig. 3a). The relative reflectance at wavelength 1410 nm in the region of likely preserved collagen in biogenic apatite is significantly lower than those of the adjacent regions of inner core and outer rim, where the relative reflectance at wavelength 1410 nm ranges from 150 to 200 (in the line plot between 0–1650 μm and 4250–4850 μm distance, see Fig. 3a). The $I(\text{C})/I(\text{Ca})$ and $I(\text{C}) \times 10/I(\text{P})$ intensity ratios of ES_SK91 follow a reverse
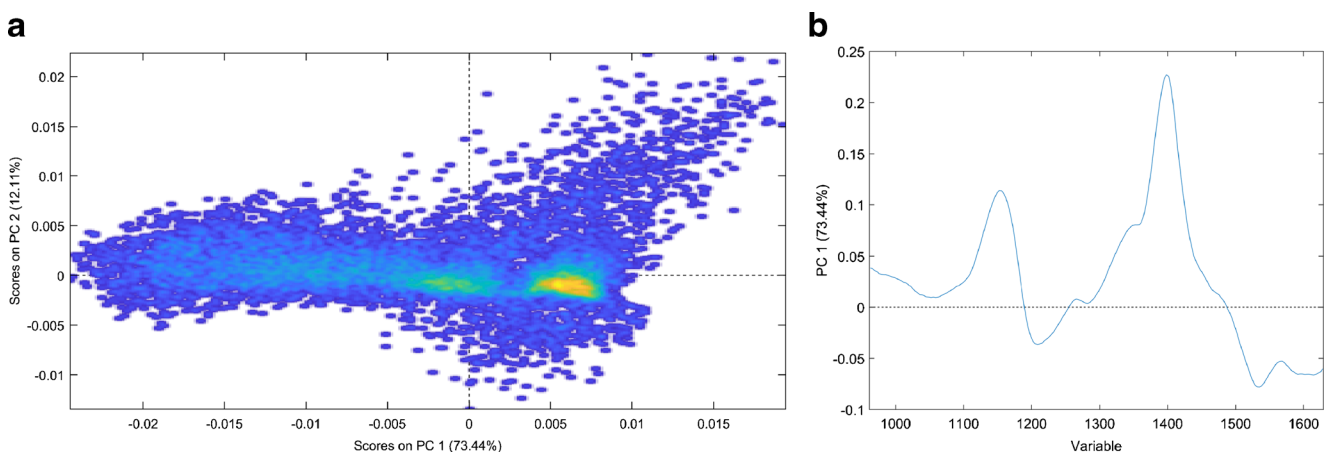

Fig. 1 (**a**) PC model scatterplot of near-infrared hyperspectral images on bone samples ES_SK91 and GT_25.05 displaying scores of PC1 against PC2; (**b**) PCA loadings on PC1 (73.44%)
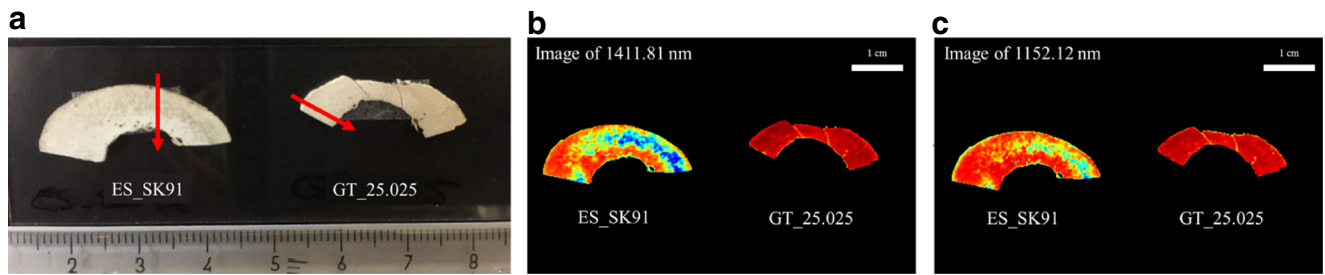
Fig. 2 (**a**) Cross sections of ES_SK91 and GT_25.025 used for NIR-HSI measurement. Red arrows indicate the position of ablation lines on mirroring cross section used for LASS ICP-QMS/MC ICP-MS measurements. (**b**) PC1 reconstructed image slabs of relative reflectance at wavelength 1410 nm for bone samples ES_SK91 and GT_25.025 (red, high relative reflectance; blue, low relative reflectance). (**c**) PC1 reconstructed image slabs of relative reflectance at wavelength 1150 nm for bone samples ES_SK91 and GT_25.025 (red, high relative reflectance; blue, low relative reflectance)

trend to the relative reflectance at wavelength 1410 nm, showing maximum values in the center of the bone cross section with likely preserved collagen in biogenic apatite (between 1650 and 4250 μm distance in the line plot, see Fig. 3a).

Vincke et al. [51] indicated that the relative reflectance at wavelength 1410 nm resulted from the absorption of the O–H bond, which may be linked to the carbonated crystal hydroxyapatite or its water content [51, 73]. The present data of this study (including "Sr isotope amount ratios in areas of preserved biogenic bone material") showed different results. The carbonate content ($w(C) \sim 0.07$) of hydroxyapatite [74] can be considered to be evenly distributed within the bone material which is in accordance with the observation that the $I(C)/I(Ca)$ and $I(C) \times 10/I(P)$ intensity ratios follow the same trend (see Fig. 3a). Thus, in this case, the lower relative reflectance at wavelength 1410 nm likely represents degradation of collagen in biogenic apatite, which is in agreement with observations from Stathopoulou et al. [48] and Thomas et al. [49] on recent/forensic and fossil bone samples.

Figure 3b shows the spot size-buffered line plot of the relative reflectance at wavelength 1410 nm together with the intensity ratios $I(C)/I(Ca)$ and $I(C) \times 10/I(P)$ of bone sample GT_25.025. The relative reflectance at wavelength 1410 nm remains stable over the major part of the bone cross-section area (variation between 230 and 250 from 0 to 4875 μm distance), with a slight decrease at the outer rim area (between 4875 and 5775 μm distance, down to 200). The $I(C)/I(Ca)$ and $I(C) \times 10/I(P)$ intensity ratios also remain stable throughout most of the bone cross section, as well. A reverse trend is seen when a significant increase at the outer rim area to maximum values is reached (between 4875 and 5775 μm distance, see Fig. 3b). While the high $I(C)/I(Ca)$ and $I(C) \times 10/I(P)$ intensity ratios in the outer rim area of GT_25.025 show similar levels as may be seen in the likely preserved collagen in biogenic apatite of ES_SK91, the differences in the relative reflectance at wavelength 1410 nm as seen in the image slabs (see Fig. 2b and c) and the line plots (Fig. 3a and b) indicate different sources for the high carbon content (see "Sr isotope amount ratios in areas of preserved biogenic bone material") in these regions, namely, on the one hand biogenic collagen and on the other hand precipitated secondary carbonates or adsorbed humic materials.
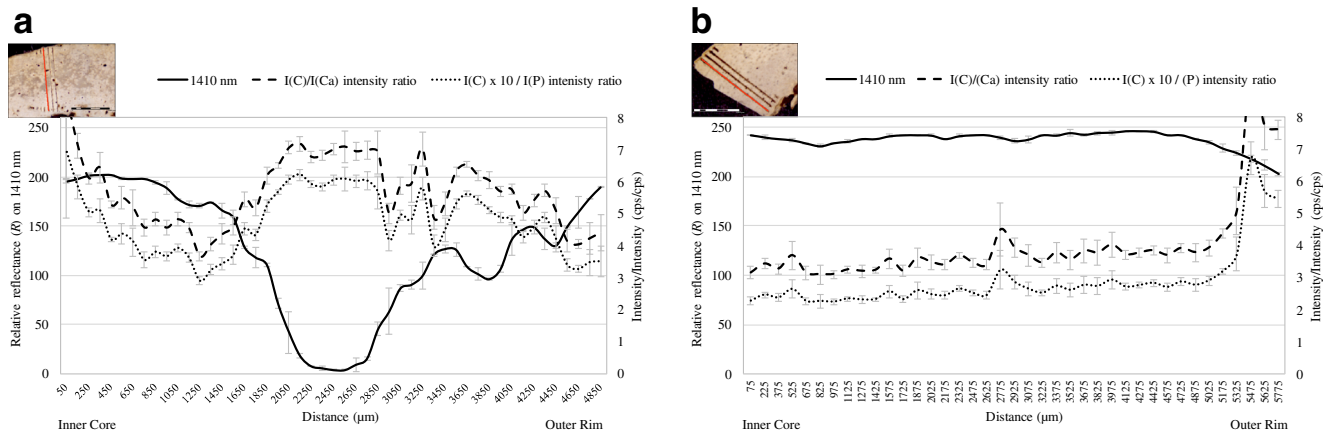

Fig. 3 Single line plot of spot size-buffered relative reflectance at wavelength 1410 nm, $I(C)/I(Ca)$ intensity ratios and $I(C) \times 10/I(P)$ intensity ratios of (**a**) ES_SK91 and (**b**) GT_25.025 in laser direction from the inner core to the outer rim. (Note that $I(C)/I(Ca)$ intensity ratios at distance of 5475 μm (9.3 cps/cps ± 0.6 cps/cps) of GT_25.025 are beyond the displayed range.) Error bars display the standard deviation over 1 spot size

## Sr isotope amount ratios in areas of preserved biogenic bone material

Bone ES_SK91: The ROIs of preserved collagen were identified in the center of the bone cross section, based on elevated $I(C)/I(Ca)$ intensity ratios (> 5 cps/cps) and $I(C) \times 10/I(P)$ (> 4.5 cps/cps) intensity ratios (see Figs. 3a, 4b–d, and Table 2). This is in agreement with recent studies from Longato et al. [46], who characterized recent/forensic bone samples as displaying a C/Ca emission ratio between 4.5 and 5.5, determined using energy-dispersive X-ray (EDS) mapping, and with recent studies from Patonai et al. [43], which characterized recent/forensic material as displaying a C × 10/P absorption ratio > 3.7, determined using FTIR analysis (see Table 2). This was confirmed by the relative reflectance at the wavelength 1410 nm (< 146, abrupt drop of relative reflectance from 150 to 8 within 600 μm (between 1650 and 2250 μm) was observed, see Figs. 3a and 4f) and histologically by visible structural differences in the microscope image. Adjacent to the ROI of preserved collagen, the ROIs of the outer rim and the inner core area were defined.

Figure 4b also shows a higher $w(Ca)/w(P)$ mass fraction ratio (average value of 2.40 μg g^{-1}/μg g^{-1} ± 0.08 μg g^{-1}/μg g^{-1} (SD), see ESM Table S3) in the area of preserved collagen in comparison to the surrounding areas of the inner

core and outer rim, which overlaps with the mass fraction ratio to be expected in human bones (2.0 μg g^{-1}/μg g^{-1} ± 0.3 μg g^{-1}/μg g^{-1} (SD)) [31, 75, 76]. The $w(Sr) \times 1000/w(Ca)$ mass fraction ratios show a negative correlation with lower values in the area of preserved collagen in biogenic apatite compared to those without sufficiently preserved collagen of outer rim and inner core areas (see Fig. 4a, e, and Table 2). Since Sr tends to accumulate upon diagenesis [26], the outer rim area showing elevated $w(Sr) \times 1000/w(Ca)$ mass fraction ratios of > 2.4 μg g^{-1}/μg g^{-1} is seen as diagenetically altered and as a consequence the $n(^{87}Sr)/n(^{86}Sr)$ isotope-amount ratio, as well. Penetrating water/movement fluids driven by pore-mediated diagenesis might be the explanation for Sr accumulations in the inner bone area and surrounding the pores/vacancies (see Fig. 4a) [77]. The region of preserved collagen in biogenic apatite is seen to be the region of best preservation of biogenic Sr signatures in this case, although it needs to be taken into consideration that diagenesis affecting $n(^{87}Sr)/n(^{86}Sr)$ isotope-amount ratio (via, e.g., water fluxes) and degradation of collagen (microbial action/bio erosion) may significantly differ in extent, depending on the decomposition conditions.

The $n(^{87}Sr)/n(^{86}Sr)$ isotope-amount ratio in the area of preserved collagen is 0.70882 ± 0.00033 (SD) (see Table 2 and Fig. 4e). This value is in agreement with the biogenic $n(^{87}Sr)/$

ES_S19K
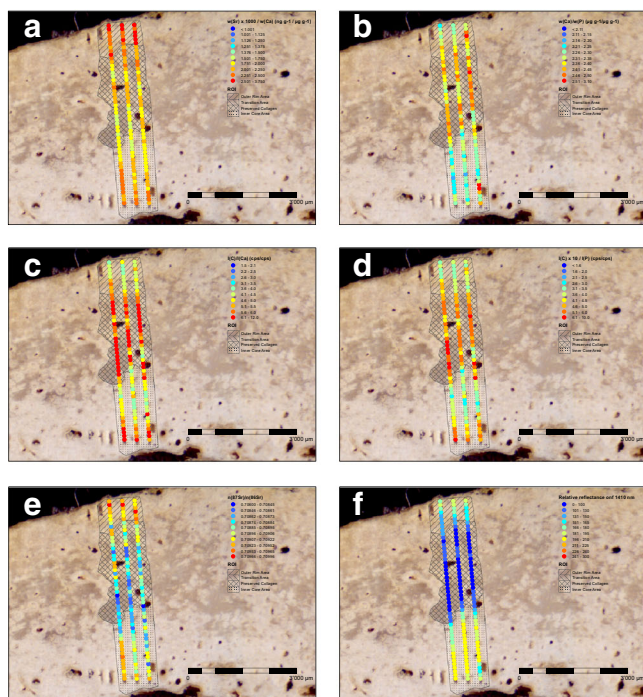
GT_25.025

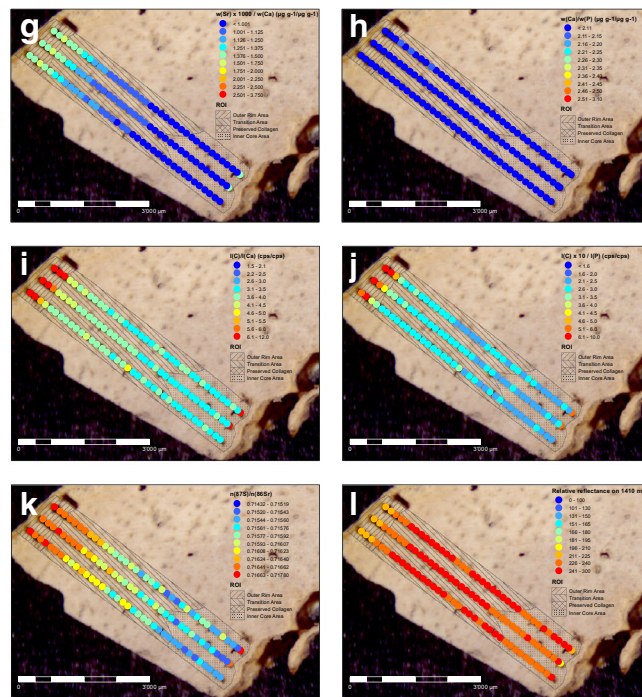**Fig. 4** Chemical imaging results for ES_SK91 displaying (**a**) $w(Sr) \times 1000/w(Ca)$ mass fraction ratios, (**b**) $w(Ca)/w(P)$ mass fraction ratios, (**c**) $I(C)/I(Ca)$ intensity ratios, (**d**) $I(C) \times 10/I(P)$ intensity ratios, (**e**) $n(^{87}Sr)/n(^{86}Sr)$ isotope-amount ratios, (**f**) relative reflectance at wavelength 1410 nm; and chemical imaging results for GT_25.025 displaying

(**g**) $w(Sr) \times 1000/w(Ca)$ mass fraction ratios, (**h**) $w(Ca)/w(P)$ mass fraction ratios, (**i**) $I(C)/I(Ca)$ intensity ratios, (**j**) $I(C) \times 10/I(P)$ intensity ratios, (**k**) $n(^{87}Sr)/n(^{86}Sr)$ isotope-amount ratios, (**l**) relative reflectance at wavelength 1410 nm. ES_SK91, GT_25.025

Table 2 Distribution of $I(C)/I(Ca)$ intensity ratios, $I(C) \times 10/I(P)$ intensity ratios, $w(Sr) \times 1000/w(Ca)$ mass fraction ratios, $n(^{87}Sr)/n(^{86}Sr)$ isotope-amount ratios, and relative reflectance at wavelength 1410 nm in the different ROIs (outer rim area, preserved collagen, transition area, inner core area) of ES_SK91 and GT_25.025 given as mean (± SD). Reference values from C/Ca emission ratio (EDS) and C × 10/P absorption ratio (FTIR)

Sample ID	ROI	$I(C)/I(Ca)$ intensity ratio (cps/cps)	$I(C) \times 10/I(P)$ intensity ratio (cps/cps)	$w(Sr) \times 1000/w(Ca)$ (ng g^{-1}/µg g^{-1})	$n(^{87}Sr)/n(^{86}Sr)$ isotope-amount ratio	Relative reflectance on 1410 nm
ES_SK91	Inner core	5.0 ± 1.2	4.0 ± 1.0	2.07 ± 0.21	0.70900 ± 0.00038	191 ± 14
	Preserved collagen	5.80 ± 0.98	4.92 ± 0.90	1.99 ± 0.20	0.70882 ± 0.00033	85 ± 36
	Outer rim	4.52 ± 0.61	3.77 ± 0.59	2.55 ± 0.26	0.70932 ± 0.00039	163 ± 19
GT_25.025	Inner core	3.32 ± 0.24	2.41 ± 0.23	0.89 ± 0.04	0.71556 ± 0.00038	238.1 ± 2.7
	Transition	3.71 ± 0.39	2.71 ± 0.31	1.12 ± 0.17	0.71603 ± 0.00046	242.8 ± 4.1
	Outer rim	7.6 ± 1.8	5.5 ± 1.3	1.49 ± 0.05	0.71664 ± 0.00032	220.7 ± 6.8
Sample type		C/Ca emission ratio (EDS)	C × 10/P absorption ratio (FTIR)			
Recent/forensic		4.5–5.5	> 3.7			
Archeological/diagenetically altered		< 4	< 3.4			
Reference		[46]	[43]			

$n(^{86}Sr)$ isotope-amount ratio of 0.70883 ± 0.00017, determined using solubility profiling (see Table 3). As the bone was recovered intact from the archeological site, only its outer surface was exposed primarily to the repository material where diagenesis is more likely. The outer rim area of the bone has a $n(^{87}Sr)/n(^{86}Sr)$ isotope-amount ratio of 0.70932 ± 0.00039 (SD) (see Table 2 and Fig. 4e). This value is in agreement with the value of the likely diagenetic fluoride-apatite [32] in the leaching residue (0.70896 ± 0.00017 (U, $k = 2$)) (see Table 3).

Bone GT_25.025: In the case of bone cross section GT_25.025, the hyperspectral data did not reveal areas of sufficiently preserved collagen. The ROI of the outer rim area was identified based on the relative reflectance at wavelength 1410 nm (< 230), by elevated $I(C)/I(Ca)$ intensity ratios (> 4) and elevated $I(C) \times 10/I(P)$ intensity ratios (> 3.6). Herein, a decrease of the relative reflectance at wavelength 1410 nm from $242.0 \pm < 0.1$ (SD) to a minimum level of 203.0 ± 1.7 (SD) over 1340 µm (between 4725 and 5775 µm distance) was observed (see Figs. 3b and 4l). For $I(C)/I(Ca)$ intensity ratios, a significant increase from 3.93 cps/cps ± 0.25 cps/cps (SD) up to 7.61 cps/cps ± 0.30 cps/cps (SD) within 750 µm (between 5025 and 5775 µm distance) was observed (see Figs. 3b and 4i). In case of $I(C) \times 10/I(P)$ intensity ratios, a significant increase of the intensity ratio from 2.92 cps/cps ± 0.14 cps/cps to 5.46 cps/cps ± 0.27 cps/cps within 750 µm (between 5025 and 5775 µm distance) was observed (see Figs. 3b and 4j). The ROI of the inner core area was estimated as the innermost homogeneous region. This was identified based on the relative reflectance on wavelength 1410 nm (< 240) and on stable $w(Sr) \times 1000/w(Ca)$ mass fraction ratios, $I(C)/I(Ca)$ intensity ratios (average 3.32 cps/cps ± 0.24 cps/cps (SD)) and $I(C) \times 10/I(P)$ intensity ratios (average 2.41 cps/cps ± 0.23 cps/cps (SD)) (see Table 2). The ROI of the transition area displays the region between the outer rim and inner core with stable relative reflectance on wavelength 1410 nm (average 242.8 ± 4.1 (SD)), stable $I(C)/I(Ca)$ intensity ratios (average 3.71 cps/cps ± 0.39 cps/cps (SD)) and $I(C) \times 10/I(P)$ intensity ratios (average 2.71 cps/cps ± 0.31 cps/cps (SD)) (see Table 2). The latter two indicate no preservation of collagen due to degradation of organic matter, which is in agreement with C/Ca emission ratio < 4 [46] and C × 10/P absorption ratio < 3.4 [43] found for archeological samples (see Table 2).

The elemental and Sr isotopic images of bone sample GT_25.025 display a clear diagenetic gradient from the outer rim area to the inner core area for $I(C)/I(Ca)$ intensity ratios (7.6 cps/cps ± 1.8 cps/cps (SD) to 3.32 cps/cps ± 0.24 cps/cps (SD), $I(C) \times 10/I(P)$ intensity ratios (5.5 cps/cps ± 1.3 cps/cps (SD) to 2.41 cps/cps ± 0.23 cps/cps (SD)), $w(Sr) \times 1000/w(Ca)$ mass fraction ratios (1.49 µg g^{-1}/µg g^{-1} ± 0.05 µg g^{-1}/µg g^{-1} (SD) to 0.89 µg g^{-1}/µg g^{-1} ± 0.04 µg g^{-1}/µg g^{-1} (SD)), and $n(^{87}Sr)/n(^{86}Sr)$ isotope-amount ratios (0.71664 ± 0.00032 (SD) to 0.71556 ± 0.00038 (SD)) (see Table 2, Fig. 4g–k).

Table 3 Diagenetic, biogenic, and residual diagenetic $n(^{87}Sr)/n(^{86}Sr)$ isotope-amount ratios of ES_SK91 and GT_25.025, determined by solubility profiling. Errors are given as combined uncertainties (U, $k = 2$)

	Initial diagenetic $n(^{87}Sr)/n(^{86}Sr)$*	Pooled leachate numbers	Biogenic $n(^{87}Sr)/n(^{86}Sr)$	Pooled leachate numbers	Residual diagenetic $n(^{87}Sr)n(^{86}Sr)$**	Pooled leachate numbers
ES_SK91	0.70858 ± 0.00017	1–2	0.70883 ± 0.00017	7–11	0.70896 ± 0.00017	Solid residue
GT_25.025	0.71686 ± 0.00018	1–2	0.71504 ± 0.00017	11	0.71527 ± 0.00017	Solid residue

*Average of the first two leachates, containing diagenetic bioapatite from secondary minerals and surface absorption

**Likely diagenetic fluoride-apatite in solid residual [32]

The $I(C)/I(Ca)$ and $I(C) \times 10/I(P)$ intensity ratios show a non-linear trend with a significant decrease within the outermost 750 μm (outer rim area) (Fig. 4i, j, ESM Fig. S2a), indicating an accumulation of C. The most significant source of C in diagenetically unaltered bones is collagen. Since collagen was not detected by the hyperspectral imaging data, it might be more likely that the source of this accumulated C is diagenesis. The increase in $I(C)/I(Ca)$ and $I(C) \times 10/I(P)$ intensity ratios points toward replacement of apatite with carbonates [26] or adsorption of organic matter (e.g., humic material). Comparison with the microscopic image after laser ablation shows a deeper ablation depth in this area, despite unchanging ablation settings, confirming a change of the tissue density.

The $w(Sr) \times 1000/w(Ca)$ mass fraction ratios follow a linear trend of decreasing diagenetic impact from the outer rim toward the inner core area (see Fig. 4g, k, ESM Fig. S2b), supporting the assumption of only one diagenetic source (i.e., repository material) (see ESM Discussion).

As the femur was recovered completely intact, we assume that only its outer surface was exposed to the repository material. Even though water/movement fluids may penetrate the inner bone via pores and vacancies [77], diagenesis is likely to affect the outer bone area to a greater extent. This indicates that the higher $n(^{87}Sr)/n(^{86}Sr)$ isotope-amount ratio in the outer rim area (0.71661 ± 0.00038 (SD)) (see Table 2) is the result of a diagenetic alteration, which is similar to the results of the solubility profiling. The initial leachates (containing large amounts of diagenetically altered material) had $n(^{87}Sr)/n(^{86}Sr)$ isotope-amount ratio values of 0.71686 ± 0.00018 (U, $k = 2$) (see Table 3). Based on the diagenetic gradient, the inner core area most likely provides the closest approximation of the biogenic Sr signature (0.71557 ± 0.00039 (SD)) (see Table 2). This value overlaps within uncertainty with the $n(^{87}Sr)/n(^{86}Sr)$ isotope-amount ratio of the biogenic material assessed by solubility profiling. The data indicates that diagenetic overprint of the Sr signatures is still present, but the current methods recovered a tendency toward the biogenic $n(^{87}Sr)/n(^{86}Sr)$ signals of this sample, which, in an archeological context, may at least enable ruling out certain areas as regions of origin.

Conclusion

The combination of NIR-HSI and LASS ICP-QMS/MC ICP-MS has been successfully applied to reveal regions of preserved collagen (generally innermost areas of the bone less affected), bearing biogenic $n(^{87}Sr)/n(^{86}Sr)$ isotope-amount ratio signatures in archeological bone samples, which are indispensable for a reliable evaluation of (pre-)historic migration (paths) during the most recent time prior to death of an individual. The application of combining the change in C content, the $w(Ca)/w(P)$ and $w(Sr) \times 1000/w(Ca)$ mass fraction ratios along with the NIR wavelengths of 1150 nm and 1410 nm, proved most useful for direct analysis of archeological bone samples using solid sample introduction such as laser ablation. The statistical combination of the obtained information allowed for the identification of biogenic areas of the bone material with a high probability. Especially the combination $I(C)/I(Ca)$ and/or $I(C) \times 10/I(P)$ intensity ratios, NIR-HSI results at the wavelength of 1410 nm and microscopic characterization allow for the detection of areas with preserved collagen in biogenic apatite. As a result, these areas can be used for the assessment of the biogenic $n(^{87}Sr)/n(^{86}Sr)$ isotope-amount ratios. In case of archeological bones with no sufficiently reserved collagen, diagenetic gradients of $w(Sr) \times 1000/w(Ca)$ mass fraction ratios, $n(^{87}Sr)/n(^{86}Sr)$ isotope-amount ratios, $I(C)/I(Ca)$ and/or $I(C) \times 10/I(P)$ intensity ratios in combination with NIR-HSI results at the wavelength of 1410 nm indicate the regions of less affected material with the best estimation of biogenic $n(^{87}Sr)/n(^{86}Sr)$ isotope-amount ratios. Herein, a diagenetic overprint cannot be fully excluded and impedes the assessment of biogenic $n(^{87}Sr)/n(^{86}Sr)$ isotope-amount ratios in archeological bone samples. In such cases, acid buffer sequential leaching may reveal biogenic $n(^{87}Sr)/n(^{86}Sr)$ isotope-amount ratios in powdered bone samples or the closest approximation of these in case of extensive diagenetic alterations, but in significantly diagenetically altered bones, biogenic bone $n(^{87}Sr)/n(^{86}Sr)$ isotope-amount ratios remain irretrievable.

Nevertheless, the present method adds a new value to bones in migration studies: Samples, which have been dismissed so far as "too diagenetically altered," may now be of use and add valuable information to the sole use of tooth enamel.

Compliance with ethical standards

Conflict of interest The authors declare that they have no conflict of interest.

Publisher's Note Springer Nature remains neutral with regard to jurisdictional claims in published maps and institutional affiliations.

References

1. Bentley RA. Strontium isotopes from the earth to the archaeological skeleton: a review. J Archaeol Method Theory. 2006;13(3):135–87.

2. Slovak NM, Paytan A. Applications of Sr isotopes in archaeology. In: Baskaran M, editor. Handbook of environmental isotope geochemistry, vol. I. Berlin, Heidelberg: Springer; 2012. p. 743–68. https://doi.org/10.1007/978-3-642-10637-8_35.

3. Szostek K, Mądrzyk K, Cienkosz-Stepańczak B. Strontium isotopes as an indicator of human migration—easy questions, difficult answers. Anthropol Rev. 2015;78(2):133–56. https://doi.org/10.1515/anre-2015-0010.

4. Sehrawat JS, Kaur J. Role of stable isotope analyses in reconstructing past life-histories and the provenancing human skeletal remains: a review. Anthropol Rev. 2017;80(3):243–58. https://doi.org/10.1515/anre-2017-0017.

5. Prohaska T, Latkoczy C, Schultheis G, Teschler-Nicola M, Stingeder G. Investigation of Sr isotope ratios in prehistoric human bones and teeth using laser ablation ICP-MS and ICP-MS after Rb/Sr separation. J Anal At Spectrom. 2002;17(8):887–91. https://doi.org/10.1039/b203314c.

6. Prohaska T, Teschler-Nicola M, Galler G, Přichystal A, Stingeder G, Jelenc M, et al. Non-destructive determination of 87Sr/86Sr isotope ratios in early upper Paleolithic human teeth from the Mladeč caves—preliminary results. In: Teschler-Nicola M, editor. Early modern humans at the Moravian Gate. Vienna: Springer-Verlag; 2006. p. 505–14. https://doi.org/10.1007/978-3-211-49294-9_18.

7. Horstwood MSA, Evans JA, Montgomery J. Determination of Sr isotopes in calcium phosphates using laser ablation inductively coupled plasma mass spectrometry and their application to archaeological tooth enamel. Geochim Cosmochim Acta. 2008;72(23):5659–74. https://doi.org/10.1016/j.gca.2008.08.016.

8. Simonetti A, Buzon MR, Creaser RA. In-situ elemental and Sr isotope investigation of human tooth enamel by laser ablation-(MC)-ICP-MS: successes and pitfalls. Archaeometry. 2008;50(2): 371–85. https://doi.org/10.1111/j.1475-4754.2007.00351.x.

9. Copeland SR, Sponheimer M, Lee-Thorp JA, le Roux PJ, de Ruiter DJ, Richards MP. Strontium isotope ratios in fossil teeth from South Africa: assessing laser ablation MC-ICP-MS analysis and the extent of diagenesis. J Archaeol Sci. 2010;37(7):1437–46. https://doi.org/10.1016/j.jas.2010.01.003.

10. Montgomery J, Evans JA, Horstwood MSA. Evidence for long-term averaging of strontium in bovine enamel using TIMS and LA-MC-ICP-MS strontium isotope intra-molar profiles. Environ Archaeol. 2010;15(1):32–42. https://doi.org/10.1179/146141010x12640787648694.

11. Le Roux PJ, Lee-Thorp JA, Copeland SR, Sponheimer M, de Ruiter DJ. Strontium isotope analysis of curved tooth enamel surfaces by laser-ablation multi-collector ICP-MS. Palaeogeogr Palaeoclimatol Palaeoecol. 2014;416:142–9. https://doi.org/10.1016/j.palaeo.2014.09.007.

12. Lewis J, Coath CD, Pike AWG. An improved protocol for 87Sr/86Sr by laser ablation multi-collector inductively coupled plasma mass spectrometry using oxide reduction and a customised plasma interface. Chem Geol. 2014;390:173–81. https://doi.org/10.1016/j.chemgeo.2014.10.021.

13. Capo RC, Stewart BW, Chadwick OA. Strontium isotopes as tracers of ecosystem processes: theory and methods. Geoderma. 1998;82:197–225.

14. Coplen TB. Guidelines and recommended terms for expression of stable-isotope-ratio and gas-ratio measurement results. Rapid Commun Mass Spectrom. 2011;25(17):2538–60. https://doi.org/10.1002/rcm.5129.

15. Blum JD, Taliaferro EH, Weisse MT, HR T. Changes in Sr/Ca, Ba/Ca and 87Sr/86Sr ratios between two forest ecosystems in the northeastern USA. Biogeochemistry. 2000;49:87–101.

16. Sealy JC, van der Merwe NJ, Sillen A, Kruger FJ, Krueger HW. 87Sr86Sr as a dietary indicator in modern and archaeological bone. J Archaeol Sci. 1991;18(3):399–416. https://doi.org/10.1016/0305-4403(91)90074-Y.

17. Grupe G, Price TD, Schröter P, Söllner F, Johnson CM, Beard BL. Mobility of Bell Beaker people revealed by strontium isotope ratios of tooth and bone: a study of southern Bavarian skeletal remains. Appl Geochem. 1997;12:517–25.

18. Lee-Thorp J, Sponheimer M. Three case studies used to reassess the reliability of fossil bone and enamel isotope signals for paleodietary studies. J Anthropol Archaeol. 2003;22(3):208–16. https://doi.org/10.1016/s0278-4165(03)00035-7.

19. Schweissing MM, Grupe G. Stable strontium isotopes in human teeth and bone: a key to migration events of the late Roman period in Bavaria. J Archaeol Sci. 2003;30(11):1373–83. https://doi.org/10.1016/S0305-4403(03)00025-6.

20. Tütken T, Vennemann TW, Pfretzschner H-U. Nd and Sr isotope compositions in modern and fossil bones—proxies for vertebrate provenance and taphonomy. Geochim Cosmochim Acta. 2011;75(20):5951–70. https://doi.org/10.1016/j.gca.2011.07.024.

21. Ortega LA, Guede I, Zuluaga MC, Alonso-Olazabal A, Murelaga X, Niso J, et al. Strontium isotopes of human remains from the San Martín de Dulantzi graveyard (Alegría-Dulantzi, Álava) and population mobility in the Early Middle Ages. Quat Int. 2013;303:54–63. https://doi.org/10.1016/j.quaint.2013.02.008.

22. Hoogewerff J, Papesch W, Kralik M, Berner M, Vroon P, Miesbauer H, et al. The last domicile of the iceman from Hauslabjoch: a geochemical approach using Sr, C and O isotopes and trace element signatures. J Archaeol Sci. 2001;28(9):983–9. https://doi.org/10.1006/jasc.2001.0659.

23. Wilson L, Pollard M. Here today, gone tomorrow? Integrated experimentation and geochemical modeling in studies of archaeological diagenetic change. Acc Chem Res. 2002;35(8): 644–51.

24. Nelson B, Deniro MJ, Schoeninger MJ, De Paolo DJ. Effects of diagenesis on strontium, carbon, nitrogen and oxygen concentration and isotopic composition of bone. Geochim Cosmochim Acta. 1986;50:1941.

25. Kohn MJ, Schoeninger MJ, Barker WW. Altered states: effects of diagenesis on fossil tooth chemistry. Geochim Cosmochim Acta. 1999;63(18):2737–47.

26. Nielsen-Marsh CM, Hedges REM. Patterns of diagenesis in bone I: the effects of site environments. J Archaeol Sci. 2000;27(12):1139–50. https://doi.org/10.1006/jasc.1999.0537.

27. Hoppe KA, Koch PL, Furutani TT. Assessing the preservation of biogenic strontium in fossil bones and tooth enamel. Int J Osteoarchaeol. 2003;13(1–2):20–8. https://doi.org/10.1002/oa.663.

28. Kyle JH. Effect of post-burial contamination on the concentrations of major and minor elements in human bones and teeth—the implications for palaeodietary research. J Archaeol Sci. 1986;13(5):403–16. https://doi.org/10.1016/0305-4403(86)90011-7.

29. Driessens FCM, Verbeeck RK. Biominerals. Boca Raton: CRC Press; 1990.

30. Lambert JB, Xue L, Buikstra JE. Physical removal of contaminative inorganic material from buried human bone. J Archaeol Sci. 1989;16(4):427–36. https://doi.org/10.1016/0305-4403(89)90017-4.

31. Price TD, Blitz J, Burton J, Ezzo JA. Diagenesis in prehistoric bone: problems and solutions. J Archaeol Sci. 1992;19(5):513–29.

32. Sillen A. Biogenic and diagenetic Sr/Ca in Plio-Pleistocene fossils of the Omo Shungura Formation. Paleobiology. 1986;12(3):311–23.

33. Reynard B, Balter V. Trace elements and their isotopes in bones and teeth: diet, environments, diagenesis, and dating of archeological and paleontological samples. Palaeogeogr Palaeoclimatol Palaeoecol. 2014;416:4–16. https://doi.org/10.1016/j.palaeo.2014.07.038.

34. Trueman CN, Palmer MR, Field J, Privat K, Ludgate N, Chavagnac V, et al. Comparing rates of recrystallisation and the potential for preservation of biomolecules from the distribution of trace elements in fossil bones. Comptes Rendus Palevol. 2008;7(2):145–58. https://doi.org/10.1016/j.crpv.2008.02.006.

35. Koenig AE, Rogers RR, Trueman CN. Visualizing fossilization using laser ablation–inductively coupled plasma–mass spectrometry maps of trace elements in Late Cretaceous bones. Geology. 2009;37(6):511–4. https://doi.org/10.1130/G25551A.1.

36. Fernandes R, Hüls M, Nadeau M-J, Grootes PM, Garbe-Schönberg CD, Hollund HI, et al. Assessing screening criteria for the radiocarbon dating of bone mineral. Nucl Inst Methods Phys Res B. 2013;294(Supplement C):226–32. https://doi.org/10.1016/j.nimb.2012.03.032.

37. Benson A, Kinsley L, Willmes M, Defleur A, Kokkonen H, Mussi M, et al. Laser ablation depth profiling of U-series and Sr isotopes in human fossils. J Archaeol Sci. 2013;40(7):2991–3000. https://doi.org/10.1016/j.jas.2013.02.028.

38. Willmes M, Kinsley L, Moncel MH, Armstrong RA, Aubert M, Eggins S, et al. Improvement of laser ablation in situ micro-analysis to identify diagenetic alteration and measure strontium isotope ratios in fossil human teeth. J Archaeol Sci. 2016;70:102–16. https://doi.org/10.1016/j.jas.2016.04.017.

39. Shemesh A. Crystallinity and diagenesis of sedimentary apatites. Geochim Cosmochim Acta. 1990;54(9):2433–8.

40. Weiner S, Bar-Yosef O. States of preservation of bones from prehistoric sites in the Near East: a survey. J Archaeol Sci. 1990;17(2):187–96. https://doi.org/10.1016/0305-4403(90)90058-D.

41. Greene EF, Tauch S, Webb E, Amarasiriwardena D. Application of diffuse reflectance infrared Fourier transform spectroscopy (DRIFTS) for the identification of potential diagenesis and crystallinity changes in teeth. Microchem J. 2004;76(1):141–9. https://doi.org/10.1016/j.microc.2003.11.006.

42. Fernández-Jalvo Y, Andrews P, Pesquero D, Smith C, Marín-Monfort D, Sánchez B, et al. Early bone diagenesis in temperate environments. Palaeogeogr Palaeoclimatol Palaeoecol. 2010;288(1–4):62–81. https://doi.org/10.1016/j.palaeo.2009.12.016.

43. Patonai Z, Maasz G, Avar P, Schmidt J, Lorand T, Bajnoczky I, et al. Novel dating method to distinguish between forensic and archeological human skeletal remains by bone mineralization indexes. Int J Legal Med. 2012;127(2):529–33. https://doi.org/10.1007/s00414-012-0785-4.

44. Gutierrez MA. Bone diagenesis and taphonomic history of the Paso Otero 1 Bone Bed, Pampas of Argentina. J Archaeol Sci. 2001;28(12):1277–90. https://doi.org/10.1006/jasc.2000.0648.

45. Boskey AL, Moore DJ, Amling M, Canalis E, Delany AM. Infrared analysis of the mineral and matrix in bones of osteonectin-null mice and their wildtype controls. J Bone Miner Res. 2009;18(6):1005–11. https://doi.org/10.1359/jbmr.2003.18.6.1005.

46. Longato S, Woss C, Hatzer-Grubwieser P, Bauer C, Parson W, Unterberger SH, et al. Post-mortem interval estimation of human skeletal remains by micro-computed tomography, mid-infrared microscopic imaging and energy dispersive X-ray mapping. Anal Methods. 2015;7(7):2917–27. https://doi.org/10.1039/c4ay02943g.

47. Woess C, Unterberger SH, Roider C, Ritsch-Marte M, Pemberger N, Cemper-Kiesslich J, et al. Assessing various infrared (IR) microscopic imaging techniques for post-mortem interval evaluation of human skeletal remains. PLoS One. 2017;12(3):e0174552. https://doi.org/10.1371/journal.pone.0174552.

48. Stathopoulou ET, Psycharis V, Chryssikos GD, Gionis V, Theodorou G. Bone diagenesis: new data from infrared spectroscopy and X-ray diffraction. Palaeogeogr Palaeoclimatol Palaeoecol. 2008;266(3–4):168–74. https://doi.org/10.1016/j.palaeo.2008.03.022.

49. Thomas D, McGoverin C, Chinsamy A, Manley M. Near infrared analysis of fossil bone from the Western Cape of South Africa. J Near Infrared Spectrosc. 2011;19(3):151–9.

50. Linderholm J, Fernández Pierna J, Vincke D, Dardenne P, Baeten V. Identification of fragmented bones and their state of preservation by using near infrared hyperspectral image analysis. J Near Infrared Spectrosc. 2013;21(6):459. https://doi.org/10.1255/jnirs.1082.

51. Vincke D, Miller R, Stassart E, Otte M, Dardenne P, Collins M, et al. Analysis of collagen preservation in bones recovered in archaeological contexts using NIR hyperspectral imaging. Talanta. 2014;125:181–8. https://doi.org/10.1016/j.talanta.2014.02.044.

52. Koehler FW, Lee IE, Kidder LH, Lewis EN. Near infrared spectroscopy: the practical chemical imaging solution. Spectrosc Eur. 2002;14(3).

53. Doneus M, Verhoeven G, Atzberger C, Wess M, Ruš M. New ways to extract archaeological information from hyperspectral pixels. J Archaeol Sci. 2014;52:84–96. https://doi.org/10.1016/j.jas.2014.08.023.

54. ElMasry G, Sun D-W. CHAPTER 1 - principles of hyperspectral imaging technology. In: Sun D-W, editor. Hyperspectral imaging for food quality analysis and control. San Diego: Academic; 2010. p. 3–43. https://doi.org/10.1016/B978-0-12-374753-2.10001-2.

55. Firtha F. Argus hyperspectral acquisition software. 2010.

56. Prohaska T, Irrgeher J, Zitek A. Simultaneous multi-element and isotope ratio imaging of fish otoliths by laser ablation split stream ICP-MS/MC ICP-MS. J Anal At Spectrom. 2016;31(8):1612–21. https://doi.org/10.1039/c6ja00087h.

57. Brand WA, Coplen TB, Vogl J, Rosner M, Prohaska T. Assessment of international reference materials for isotope-ratio analysis (IUPAC technical report). Pure Appl Chem. 2014;86(3):425–67. https://doi.org/10.1515/pac-2013-1023.

58. Galler P, Limbeck A, Boulyga SF, Stingeder G, Hirata T, Prohaska T. Development of an on-line flow injection Sr/ matrix separation method for accurate, high-throughput determination of Sr isotope ratios by multiple collector-inductively coupled plasma-mass spectrometry. Anal Chem. 2007;79:5023–9.

59. Galler P, Limbeck A, Uveges M, Prohaska T. Automation and miniaturization of an on-line flow injection Sr/matrix separation method for accurate, high throughput determination of Sr isotope ratios by MC-ICP-MS. J Anal At Spectrom. 2008;23(10):1388. https://doi.org/10.1039/b803964j.

60. Romaniello SJ, Field MP, Smith HB, Gordon GW, Kim MH, Anbar AD. Fully automated chromatographic purification of Sr and Ca for isotopic analysis. J Anal At Spectrom. 2015;30(9):1906–12. https://doi.org/10.1039/c5ja00205b.

61. Woodhead J, Swearer S, Hergt J, Maas R. In situ Sr-isotope analysis of carbonates by LA-MC-ICP-MS: interference corrections, high spatial resolution and an example from otolith studies. J Anal At Spectrom. 2005;20(1):22. https://doi.org/10.1039/b412730g.

62. Irrgeher J, Galler P, Prohask T. 87Sr/86Sr isotope ratio measurements by laser ablation multicollector inductively coupled plasma mass spectrometry: reconsidering matrix interferences in bioapatites and biogenic carbonates. Spectrochim Acta B. 2016;125:31–42. https://doi.org/10.1016/j.sab.2016.09.008.

63. Draxler J, Zitek A, Meischel M, Stranzl-Tschegg SE, Mingler B, Martinelli E, et al. Regionalized quantitative LA-ICP-MS imaging of the biodegradation of magnesium alloys in bone tissue. J Anal At Spectrom. 2015. https://doi.org/10.1039/C5JA00354G10.1039/c5ja00354g.

64. Zitek A, Aleon J, Prohaska T. CHAPTER 9 chemical imaging. In: Prohaska T, Irrgeher J, Zitek A, Jakubowski N, editors. Sector field mass spectrometry for elemental and isotopic analysis: The Royal Society of Chemistry; 2015. p. 152–82. https://doi.org/10.1039/9781849735407-00152.

65. Schultheiss G. Analysis of isotope ratios in anthropological and archaeological samples by high resolution inductively coupled plasma mass spectrometry (HR-ICP-MS). Vienna: University of Natural Resources and Life Sciences; 2003.

66. Theiner S. The use of strontium isotope ratio measurements by MC-ICP-MS for fundamental studies on diagenesis and for the reconstruction of animal migration at the Celtic excavation site Roseldorf Diplomarbeit. Vienna: University of Vienna; 2011.

67. Swoboda S, Brunner M, Boulyga SF, Galler P, Horacek M, Prohaska T. Identification of Marchfeld asparagus using Sr isotope

68. Irrgeher J, Teschler-Nicola M, Leutgeb K, Weiß C, Kern D, Prohaska T. Migration and mobility in the latest Neolithic of the Traisen Valley, Lower Austria: Sr isotope analysis. In: Kaiser E, Burger J, Schier W, editors. Population dynamics in prehistory and early history. New approaches by using stable isotopes and genetics, vol. 5. Berlin, Boston: De Gruyter; 2012. p. 213–26. https://doi.org/10.1515/9783110266306.

69. Retzmann A, Zimmermann T, Pröfrock D, Prohaska T, Irrgeher J. A fully automated simultaneous single-stage separation of Sr, Pb, and Nd using DGA resin for the isotopic analysis of marine sediments. Anal Bioanal Chem. 2017;409(23):5463–80. https://doi.org/10.1007/s00216-017-0468-6.

70. Irrgeher J, Prohaska T, Sturgeon RE, Mester Z, Yang L. Determination of strontium isotope amount ratios in biological tissues using MC-ICPMS. Anal Methods. 2013;5(7):1687. https://doi.org/10.1039/c3ay00028a.

71. Horsky M, Irrgeher J, Prohaska T. Evaluation strategies and uncertainty calculation of isotope amount ratios measured by MC ICP-MS on the example of Sr. Anal Bioanal Chem. 2016;408(2):351–67. https://doi.org/10.1007/s00216-015-9003-9.

72. Burton JH, Price TD, Middleton WD. Correlation of bone Ba/Ca and Sr/Ca due to biological purification of calcium. J Archaeol Sci. 1999;26(6):609–16. https://doi.org/10.1006/jasc.1998.0378.

73. Osborne BG. Near-infrared spectroscopy in food analysis. In: Encyclopedia of analytical chemistry. Major reference works: Wiley; 2006. p. 1–14. https://doi.org/10.1002/9780470027318.a1018.

74. Wopenka B, Pasteris JD. A mineralogical perspective on the apatite in bone. Mater Sci Eng C. 2005;25(2):131–43. https://doi.org/10.1016/j.msec.2005.01.008.

75. White EM, Hannus LA. Chemical weathering of bone in archaeological soils. Am Antiq. 1983;48(2):316–22.

76. Tzaphlidou M, Zaichick V. Calcium, phosphorus, calcium-phosphorus ratio in rib bone of healthy humans. Biol Trace Elem Res. 2003;93(1):63–74. https://doi.org/10.1385/BTER:93:1-3:63.

77. Keenan SW. From bone to fossil: a review of the diagenesis of bioapatite. Am Mineral. 2016;101(9):1943–51. https://doi.org/10.2138/am-2016-5737.

Anika Retzmann is currently finalizing her PhD studies in analytical chemistry under the supervision of Thomas Prohaska at the University of Natural Resources and Life Sciences Vienna (BOKU), Austria. She specializes in the development of methods for elemental and isotopic analyses of biomaterials applying (laser ablation) (multiple collector) inductively coupled plasma mass spectrometry and chemical imaging techniques to address research questions related to biomedicine and archaeometry.

Magdalena Blanz is a PhD student at the Orkney Archaeology Institute, University of the Highlands and Islands, UK. Her research in archeological chemistry investigates how the analysis of skeletal remains may be improved, as well as how the consumption/use of seaweed may be identified in the archeological record.

Jörg Feldmann has been the head of TESLA (Trace Element Speciation Laboratory) at the University of Aberdeen, UK, for almost 20 years. His research focuses on speciation analysis and bioimaging of trace elements in biological and environmental samples. He has recently been awarded the 2015 European Award for Plasmaspectrochemistry; he received the 2016 RSC Interdisciplinary Prize and Medal and was elected as a Fellow of the Royal Society of Edinburgh. He is on the Advisory Board of ABC and published > 250 papers which have received over 12,000 citations.

Andreas Zitek is currently working as Scientific Project Coordinator and Lead Researcher at the new Austrian Competence Centre for Feed and Food Quality, Safety & Innovation (FFoQSI) and is associated to the Department of Chemistry, Division of Analytical Chemistry, at the University of Natural Resources and Life Sciences Vienna (BOKU), Austria. Besides applying elemental and isotopic fingerprints to identify the geographical origin of food, a special focus of his work is chemical imaging from micrometer (small compartment) to kilometer (landscape, isoscape) scale by the application of GIS methods and hyperspectral imaging in the near infrared.

Maria Teschler-Nicola is ao. Professor of (Physical) Anthropology at the University of Vienna and director retired of the Department of Anthropology and the Pathologic-Anatomical Collection at the "Narrenturm" at the Natural History Museum Vienna. She has been the leader of several research projects that focused on paleoanthropology and paleo-epidemiology and paleopathology of ancient populations of Austrian and studies concerning the (discipline) history of anthropology. Ongoing projects (supported by the EU) include contentious collections of human remains and archaeothanatology.

Johanna Irrgeher currently holds a position as Senior Scientist and Lecturer at the University of Natural Resources and Life Sciences Vienna (BOKU), Austria. She has recently completed an appointment as Post-doctoral Fellow at the Helmholtz Centre in Geesthacht, Germany. She is Chair of the Subcommittee on Isotopic Abundance Measurement of the IUPAC Commission on Isotopic Abundances and Atomic Weights (CIAAW), and her current research interests are dedicated to analytical mass spectrometry and the application of isotope tools in medical, environmental, and material sciences including the implementation of fundamental metrological methods.

Thomas Prohaska is Chair of General and Analytical Chemistry at the Montanuniversität Leoben, Austria, and specializes in the analysis of trace metals and isotope amount ratios through the application of rigorous metrological principles using advanced analytical methods based on (laser ablation) mass spectrometry and optical methods. His work demonstrates his commitment to high-quality science and education.